

Rigorous Quantum Thermodynamics from Extended Path Integral Coarse-Graining

Jing Shen,^{†,⊥} Ziyang Ye,^{†,⊥} Ming-Zheng Du,[†] Shi-Yu He,[†] Dong H. Zhang,^{‡,¶}
Venkat Kapil,^{*,§} Jia-Xi Zeng,^{*,||} and Wei Fang^{*,†}

[†]*Department of Chemistry, Shanghai Key Laboratory of Molecular Catalysis and Innovative Materials, State Key Laboratory of Porous Materials for Separation and Conversion, Fudan University, Shanghai 200438, P. R. China*

[‡]*State Key Laboratory of Molecular Reaction Dynamics, Dalian Institute of Chemical Physics, Chinese Academy of Sciences, Dalian 116023, P. R. China*

[¶]*University of Chinese Academy of Sciences, Beijing 100049, China*

[§]*Department of Physics and Astronomy, London Centre for Nanotechnology, Thomas Young Centre, University College London, WC1E 6BT London, United Kingdom*

^{||}*Dipartimento di Chimica, Università degli Studi di Milano, via Golgi 19, 20133 Milano, Italy*

[⊥]*These authors contributed equally to this work.*

E-mail: v.kapil@ucl.ac.uk; jiaxi.zeng@unimi.it; wei_fang@fudan.edu.cn

Abstract

Recent advances in machine-learning potentials have made molecular dynamics (MD) simulations increasingly predictive by enabling efficient descriptions of electronic quantum effects. However, nuclear quantum effects (NQEs) remain largely neglected due to their significant computational cost, limiting MD's ability to capture isotope effects and quantum tunnelling and leading to systematic thermodynamic errors. We extend path-integral coarse-graining (PIGS), a machine-learning approach for qualitatively incorporating NQEs, into a rigorous and accurate method for quantum thermodynamics. Specifically, this extended framework (EPIGS) enables the construction of temperature-transferable effective potentials that rigorously incorporate NQEs into classical MD simulations. Central to EPIGS is an instanton-based free-energy perturbation scheme (RPI-FEP) that provides direct and efficient estimation of the path-integral centroid potential. Benchmarks against full path-integral simulations on representative hydrogen-bonded systems, including liquid water, show that EPIGS reproduces free energies and enthalpies within 0.2 meV/atom at near-classical cost. EPIGS transforms the qualitative PIGS approach into an accurate and scalable route to quantum thermodynamic simulations in complex systems.

1 Introduction

Methodological advances in molecular dynamics (MD) have made it a cornerstone tool for studying atomic-scale processes over time, providing molecular-level insights into structure, dynamics, mechanisms, and thermodynamics. In particular, recent advances in machine-learning potentials (MLPs) have revolutionised MD by enabling large-scale simulations with *ab initio* accuracy at greatly reduced cost.¹ However, while these MLPs effectively capture the quantum mechanical behaviour of electrons to make high-fidelity *ab initio* MD practical, the overwhelming majority of such simulations continue to treat atomic nuclei as classical particles. This classical-nuclei approximation neglects nuclear quantum effects (NQEs), e.g. zero-point energy and tunnelling, leading to errors or failures in predicting isotope effects and many physical and chemical properties, especially in systems containing hydrogen.^{2,3} The crucial role of NQEs has been reported across diverse systems, from various fundamental systems, such as water and ice,⁴⁻⁹ interfacial and confined water,^{10,11} gas-phase dimers,^{12,13} molecular crystals,^{14,15} and simple organic liquids,^{16,17} to more complex or application-oriented systems, including biomolecules,¹⁸⁻²² metal organic frameworks (MOFs) for hydrogen storage or isotope separation,^{23,24} and superconducting systems,²⁵ just to name a few. Neglecting NQEs has emerged as a major source of systematic error in molecular modelling.

Imaginary time path integral methods, namely path integral molecular dynamics (PIMD) and path integral Monte Carlo (PIMC), rigorously represent quantum Boltzmann statistics by exploiting the isomorphism between a quantum particle and a classical ring polymer.²⁶ Furthermore, they enable approximate real-time quantum dynamics, most notably via ring-polymer molecular dynamics (RPMD)^{27,28} and centroid molecular dynamics (CMD)²⁹⁻³¹ methods. Although these methods are applicable to complex condensed-phase systems, simulating multiple coupled replicas of the classical system (beads) incurs substantial computational overhead, typically 1-2 orders of magnitude more costly than classical MD, due to the large number of beads required for convergence, particularly at low temperatures or

for light nuclei. Considerable effort has been devoted to reducing the cost of PIMD, with various bead-reduction strategies developed over the past decade, including coloured-noise thermostats that mimic quantum fluctuations,^{32,33} ring-polymer contraction,³⁴ and fourth-order path integral methods.³⁵ These methods can typically reduce the cost of simulating NQEs by a factor of 2-10, and have seen success in extending the capacity of PIMD for various applications.

Despite these advances, the computational overhead for path integral simulations remains substantial compared to classical MD, limiting their widespread application. Moreover, existing bead-reduction schemes each suffer from inherent deficiencies.² An alternative route for incorporating NQEs into MD is based on quantum effective potentials that modify the underlying potential energy surface, a concept that originates from the Feynman–Hibbs (FH) theory.³⁶ In fact, the FH approximation has seen applications in MD simulations of complex systems such as MOF²³ due to its great efficiency. Recent developments have revitalised this concept through machine learning. The path-integral coarse-graining (PIGS) approach leverages MLPs to learn the effective force acting on the path-integral centroid, replacing the explicit ring-polymer representation with classical MD on an NQE-corrected effective potential.^{37–40} In doing so, it provides an efficient, machine-learned realization of CMD at near-classical cost. However, because PIGS learns only forces and not the underlying centroid free-energy surface, it cannot rigorously recover quantum thermodynamic quantities and the resulting potentials lack energetic consistency. Consequently, PIGS has generally been regarded as a computationally inexpensive but approximate approach, primarily used for qualitative simulations of NQEs and approximate quantum dynamics (e.g. vibrational spectrum), rather than a true alternative to PIMD or PIMC.

In this work, we develop an instanton-based free-energy perturbation approach (RPI-FEP) to efficiently and rigorously estimate the path-integral centroid free energy. This approach extends the PIGS framework to enable the rigorous evaluation of quantum thermodynamic properties and the training of temperature-transferable CMD effective poten-

tials. We demonstrate that our extended PIGS (EPIGS) method achieves high quantitative accuracy for representative systems while retaining the computational efficiency of classical MD. EPIGS is thereby positioned as a scalable and predictive framework with the potential to supplant path-integral molecular dynamics across a broad range of applications.

2 Theory

2.1 EPIGS from the centroid formulation of the quantum partition function

In the imaginary-time path integral formulation, the quantum-mechanical partition function is isomorphic to the partition function of a classical ring polymer (RP), which can be reformulated in terms of the RP centroid,^{26,30}

$$\begin{aligned}
 Z &= \left(\frac{m}{2\pi\beta_P\hbar^2} \right)^{Pf/2} \int d\mathbf{x}_1 \cdots \int d\mathbf{x}_P e^{-\beta_P U_{\text{RP}}(\mathbf{x}_1, \dots, \mathbf{x}_P)} \\
 &= \lambda^{-f} \int d\mathbf{x}_c \left[\frac{P^{Pf/2}}{\lambda^{(P-1)f}} \int d\mathbf{x}_1 \cdots \int d\mathbf{x}_P \delta_c e^{-\beta_P U_{\text{RP}}} \right] \\
 &\equiv \lambda^{-f} \int d\mathbf{x}_c e^{-\beta A_c(\mathbf{x}_c; \beta)}
 \end{aligned} \tag{1}$$

in which P is the number of beads, $\beta = 1/k_B T$ is the inverse temperature and $\beta_P = \beta/P$, f is the number of degrees of freedom, $\lambda = \sqrt{2\pi\beta\hbar^2/m}$ is the thermal de Broglie wavelength, U_{RP} is the RP potential, $\mathbf{x}_{P+1} \equiv \mathbf{x}_1$, $\delta_c \equiv \delta \left(\frac{1}{P} \sum_{i=1}^P \mathbf{x}_i - \mathbf{x}_c \right)$ constrains the RP centroid to \mathbf{x}_c , and A_c is the centroid free energy, also known as the centroid potential of mean force. For simplicity, we assume all atoms have mass m ; extending to unequal masses is straightforward using the mass-weighted coordinates.

Our EPIGS approach rigorously computes quantum thermodynamic quantities from the centroid formulation of the quantum partition function by leveraging machine learning to not only learn the centroid mean force $\mathbf{f}_c = -\frac{\partial A_c}{\partial \mathbf{x}_c}$ but also A_c . Furthermore, EPIGS en-

ables temperature-transferable centroid potentials by incorporating temperature into the descriptor and explicitly learning its derivative $\frac{\partial A_c}{\partial \beta}$. This quantity is essentially the quantum entropic term and can be evaluated from the same simulation used to obtain \mathbf{f}_c once A_c is available,

$$\beta \frac{\partial A_c}{\partial \beta} = TS_c = \left\langle \widehat{K} + \widehat{V} \right\rangle_{U_{\text{RP}}, \mathbf{x}_c} - \frac{f}{2\beta} - A_c, \quad (2)$$

where \widehat{K} is the virial kinetic energy estimator, \widehat{V} is the potential energy estimator, and the bracket denotes the centroid-constrained ensemble average under a given RP potential

$$\langle \dots \rangle_{U_a, \mathbf{x}_c} \equiv \frac{\int d\mathbf{x}_1 \dots \int d\mathbf{x}_P \delta_c(\dots) e^{-\beta_P U_a}}{\int d\mathbf{x}_1 \dots \int d\mathbf{x}_P \delta_c e^{-\beta_P U_a}}. \quad (3)$$

Without explicitly sampling the ring polymer, the quantum mechanical internal energy U^q can be computed simply from EPIGS-MD simulation,

$$U^q = -\frac{\partial \ln Z}{\partial \beta} = \frac{\int d\mathbf{x}_c \left(A_c + \beta \frac{\partial A_c}{\partial \beta} \right) e^{-\beta A_c(\mathbf{x}_c; \beta)}}{\int d\mathbf{x}_c e^{-\beta A_c(\mathbf{x}_c; \beta)}} + \frac{f}{2\beta}. \quad (4)$$

The classical to quantum free-energy shift is given by,

$$A^q - A^{\text{cl}} \equiv \Delta A^{q \leftarrow \text{cl}} = -\frac{1}{\beta} \ln \frac{\int d\mathbf{x}_c e^{-\beta A_c(\mathbf{x}_c; \beta)}}{\int d\mathbf{x}_c e^{-\beta V(\mathbf{x}_c)}}, \quad (5)$$

which can be computed via thermodynamic integration (TI) over an order parameter $\lambda \in [0, 1]$ that smoothly transforms V to A_c : $V_\lambda = V + \lambda(A_c - V)$, a procedure we denote as EPIGS-TI. The remaining two thermodynamic potentials, enthalpy H^q and Gibbs free energy G^q can be computed similarly.

While the centroid mean force \mathbf{f}_c can be obtained directly from fixed-centroid PIMD simulations,^{26,30,38} obtaining A_c is challenging. Previous PIGS implementations^{37–40} have therefore either omitted A_c entirely or approximated it by neglecting the entropic contribution. This prevents rigorous evaluation of quantum thermodynamic quantities and compromises

the energetic consistency of the learned potentials. EPIGS resolves this limitation while preserving the efficiency of the original PIGS framework. The key methodological advance enabling EPIGS is discussed in the following section.

2.2 Instanton based free-energy perturbation

One possible way to compute A_c is via TI from classical to quantum nuclei, e.g. mass-TI, [13,21,41](#) scaled-coordinates-TI, [42](#) etc. However, TI based approaches share a common issue of being computationally demanding, i.e. obtaining A_c would be around an order of magnitude more expensive than obtaining \mathbf{f}_c , rendering them impractical. Free-energy perturbation (FEP) provides an alternative route, computing the free energy difference between the true potential U_b and a reference potential U_a in one simulation, [26](#)

$$A_{c,b} - A_{c,a} = -\frac{1}{\beta} \ln \langle e^{-\beta P(U_b - U_a)} \rangle_{U_a, \mathbf{x}_c}. \quad (6)$$

The primary challenge in reliable FEP is constructing a reference potential U_a with analytically known free energy that ensures sufficient configuration-space overlap with the true potential.

We realise that the centroid constraint δ_c strongly restricts the configuration space, making the harmonic oscillator (HO) reference a reasonable choice. When the vibrational frequencies ω_j at \mathbf{x}_c satisfy $\text{Im} \omega_j < \frac{2\pi}{\beta \hbar}$, the P -bead RP free energy for the HO, [43](#) with the centroid constrained at \mathbf{x}_c , is given by

$$A_{c,\text{HO}}(\mathbf{x}_c; \beta) = \frac{1}{\beta} \sum_{j=1}^f \ln \frac{\sinh [P \sinh^{-1} (\beta_P \hbar \omega_j / 2)]}{\beta \hbar \omega_j / 2} + V(\mathbf{x}_c). \quad (7)$$

U_{RP} for this reference is quadratic and positive definite, meaning that FEP (Eq. 6) can be performed using PIMC with the Gaussian sampling protocol. However, in regimes relevant to quantum tunnelling, i.e. with large imaginary frequencies or at low temperatures, the

condition $\text{Im } \omega_j < \frac{2\pi}{\beta\hbar}$ is frequently violated, rendering the HO reference invalid.

When imaginary-frequency modes with $\text{Im } \omega_j \geq \frac{2\pi}{\beta\hbar}$ exist, the RP delocalises along these modes rather than collapsing onto its centroid, resulting in a configuration that resembles an instanton⁴⁴ describing quantum tunnelling through a barrier. Inspired by semiclassical instanton theory,^{44–47} we designed a ring-polymer-instanton (RPI)-like reference,

$$U_{\text{RPI}}(\mathbf{x}) = U_{\text{RP}}|_{\mathbf{x}^*} + \frac{1}{2}(\mathbf{x} - \mathbf{x}^*)^T \tilde{\mathbf{H}}_{\text{RP}}|_{\mathbf{x}^*} (\mathbf{x} - \mathbf{x}^*) \quad (8)$$

where $\mathbf{x} \equiv (\mathbf{x}_1, \dots, \mathbf{x}_P)$ denotes the closed imaginary-time path subject to δ_c , \mathbf{x}^* is a stationary orbit that minimises U_{RP} under δ_c , and $\tilde{\mathbf{H}}_{\text{RP}}$ is the ring-polymer Hessian with the centroid normal modes projected out. Similar to instanton theory calculations, \mathbf{x}^* can be obtained using instanton optimisation algorithms⁴⁸ with constraints. The free energy of the RPI reference can be computed analytically,

$$A_{\text{c,RPI}}(\mathbf{x}_c; \beta) = -\frac{1}{\beta} \ln \left[P^{f+1} \sqrt{\frac{B_P}{2\pi\beta_P\hbar^2}} \prod_{k=2}^{(P-1)f} \frac{1}{\beta_P\hbar\eta_k} \right] + \frac{U_{\text{RP}}|_{\mathbf{x}^*}}{P} \quad (9)$$

in which $B_P = \sum_{i=1}^P \sum_{j=1}^f m_j (x_{i+1,j}^* - x_{i,j}^*)^2$, \mathbf{e}_k and η_k are the eigenvectors and eigenvalues of the mass-weighted $\tilde{\mathbf{H}}_{\text{RP}}|_{\mathbf{x}^*}$. The product starts from $k = 2$ since $\tilde{\mathbf{H}}_{\text{RP}}$ is positive semi-definite, with a single zero mode \mathbf{e}_1 associated with permutational invariance, which is treated separately. A coordinate transformation from \mathbf{x}_i in the Cartesian basis to $(\tau_0, q_k)_{k \geq 2}$ in $\{\mathbf{e}_k(\tau_0)\}_{k \geq 2}$ basis, where $\tau_0 \in [0, \beta\hbar)$ is a permutational coordinate, allows one to integrate out all possible permutations. Consequently, sampling can be restricted to the eigenvector subspace with positive eigenvalues $\{\mathbf{e}_k\}_{k \geq 2}$, allowing FEP to be performed using PIMC with the Gaussian sampling protocol. Additionally, a weight term arising from the Jacobian determinant of the coordinate transformation needs to be included (see the Supplementary Information (SI) for the derivation). We name this method the ring-polymer instanton free-energy perturbation (RPI-FEP) method. For centroid geometries satisfying $\text{Im } \omega_j < \frac{2\pi}{\beta\hbar}$, the

RPI collapses, and $A_{c,\text{RPI}}$ returns to the HO reference (Eq. 7).

2.3 Temperature-transferable machine learning

In analogy with the Δ -learning strategy in MLPs, we train the model on the difference between the centroid free energy and the classical potential energy, $\Delta A_c(\mathbf{x}_c; \beta) \equiv A_c(\mathbf{x}_c; \beta) - V(\mathbf{x}_c)$, and the corresponding force differences, $\Delta \mathbf{f}_c(\mathbf{x}_c; \beta) \equiv \mathbf{f}_c(\mathbf{x}_c; \beta) - \mathbf{f}(\mathbf{x}_c)$, where $\mathbf{f}(\mathbf{x}_c) = -\nabla V(\mathbf{x}_c)$. ΔA_c varies smoothly with configuration and spans a substantially smaller energy range compared to the full centroid potential A_c , improving model accuracy with limited training data. We employ the MACE equivariant message-passing neural network,⁴⁹ although any MLP architecture is applicable in principle. At a fixed temperature, training an EPIGS potential follows the standard MLP procedure, using a dataset of centroid configurations \mathbf{x}_c with corresponding ΔA_c and $\Delta \mathbf{f}_c$ evaluated at the given temperature.

The temperature-transferable EPIGS model incorporates β as a continuous input via graph-level conditioning. A multilayer perceptron encodes β into a latent vector that is broadcast to all nodes prior to message passing, preserving the intensive nature of temperature (Fig. 1). This construction allows the temperature derivative $\frac{\partial A_c}{\partial \beta}$ (essentially the quantum entropic term) to be obtained directly via automatic differentiation. The total training loss function combines energy, force, and entropic matching terms (\mathcal{L}_A , \mathcal{L}_f , and \mathcal{L}_S), $\mathcal{L} = w_A \mathcal{L}_A + w_f \mathcal{L}_f + w_S \mathcal{L}_S$, where the weights (w_A , w_f and w_S) balance their relative contributions. The entropic term enforces thermodynamic consistency by coupling the learned free-energy surface to its temperature derivative, ensuring internally consistent predictions of both the centroid free energy and the quantum entropic term within a single training protocol.

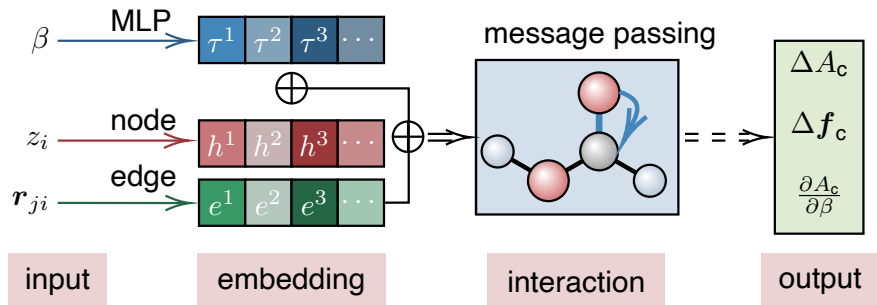


Figure 1: Schematic of temperature-dependent message-passing neural network architecture. The inverse temperature β is encoded via a multilayer perceptron into a latent embedding vector $\boldsymbol{\tau}$, which is broadcast to all atoms and concatenated (\oplus) with the node features \mathbf{h}_i (initialized from atomic numbers z_i) prior to message passing. Edge features \mathbf{e}_{ji} encode interatomic distances and directions (\mathbf{r}_{ji}). The network outputs the quantum contributions ΔA_c and $\Delta \mathbf{f}_c$, and the temperature derivative $\frac{\partial A_c}{\partial \beta}$.

3 Results

We apply the EPIGS framework to representative benchmark systems: the formic acid series (including formic acid dimer (FAD), deuterated formic acid HCOOD, and formate anion HCOO^-), the adenine–thymine (AT) base pair, and liquid water, chosen as fundamental hydrogen-bonded systems covering gas-phase clusters, biologically relevant motifs, and the condensed phase. All simulations employ the MACE-OFF23⁵⁰ foundation model as the underlying potential, fine-tuned with additional $\omega\text{B97M-D3(BJ)}/\text{def2-TZVPPD}$ ^{51,52} calculations using the ORCA⁵³ program for each system. All the computational details regarding electronic structure calculations, EPIGS potential construction, MD, EPIGS-MD, PIMD, mass-TI, and EPIGS-TI simulations and convergence tests are provided in the SI. We first benchmark the accuracy of the RPI-FEP approach for computing ΔA_c in these systems. Then we assess how well EPIGS learns the resulting centroid surfaces and evaluate its predictions of classical-to-quantum free-energy shifts and gas-phase binding and dissociation free energies, as well as the enthalpy of vaporisation of liquid water. Most calculations are performed at room temperature (300 K); temperature-transferable models are tested across 250–400 K, spanning conditions relevant to practical applications.

We first assess the performance of the RPI-FEP approach by benchmarking it against fixed-centroid mass-TI on the test systems at different temperatures. The test configurations consist of randomly selected geometries from FAD, adenine, and water clusters of varying sizes, chosen to span a range of hydrogen-bonding environments and nuclear quantum effects. Four configurations that exhibit large imaginary frequencies are selected to examine the performance of the instanton reference state. The corresponding instantons all exhibit delocalisation of a single hydrogen atom along a dominant reaction coordinate (see e.g. Fig. 2a). As shown in Fig. 2b, the RPI-FEP estimates of the centroid potential A_c are in excellent agreement with the benchmark results across all test configurations, with nearly all RPI-FEP values falling within the statistical error bars of mass-TI. Importantly, this accuracy is achieved at a dramatically reduced computational cost: while fixed-centroid mass-TI is nearly an order of magnitude more expensive than the calculation of \mathbf{f}_c , computing A_c via RPI-FEP costs much less than computing \mathbf{f}_c . These results demonstrate that the RPI-FEP approach provides a reliable and highly efficient estimate of the key quantity A_c for EPIGS.

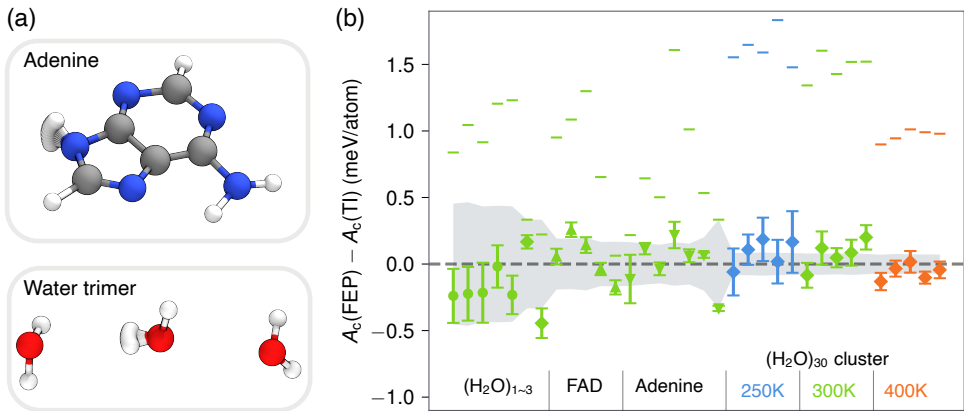


Figure 2: (a) Representative snapshots of the ring-polymer instanton configurations for adenine (top) and water trimer (bottom). (b) Benchmark of RPI-FEP against fixed-centroid mass-TI for the centroid free energy. Deviation ($A_c(\text{FEP}) - A_c(\text{TI})$) is shown for small molecules ($(\text{H}_2\text{O})_{1-3}$, FAD, adenine) at 300 K, and for 30-molecule water clusters at 250, 300, and 400 K. Horizontal dashes indicate the ring-polymer reference values, and the shaded region represents the statistical uncertainty of the mass-TI reference. System sizes range from 3 to 90 atoms.

Having established the accuracy of our approach for computing A_c , we next examine the performance of the EPIGS models trained at a single temperature. Training data were generated from PIMD trajectories by selecting 150–300 representative configurations for each species using farthest-point sampling to maximise structural diversity. No energy-based filtering was applied, so the dataset naturally spans the full range of thermally accessible configurations. For FAD and AT, the dataset includes both monomer and dimer configurations, while for HCOOD and HCOO^- , configurations are drawn from single-species trajectories. Each dataset was partitioned into training, validation, and test subsets in an approximate 8:1:1 ratio. The EPIGS models achieve excellent training accuracy across all systems (see SI), with root-mean-square errors (RMSEs) below 0.1 meV per atom for energies (except for HCOOD with a RMSE of 0.14 meV per atom) and small relative force errors (e.g., 3.8% for FAD and 5.1% for the AT base pair). The consistently low training errors confirm energy–force consistency in the training data between the centroid free energy and forces. Validation and test errors closely match training performance for both energies and forces, indicating minimal overfitting and robust generalisation. The uniform accuracy observed across chemically and structurally diverse systems highlights the broad applicability of the EPIGS framework.

Finally, we assess the performance of temperature-transferable EPIGS on liquid water, which represents the most challenging test system considered. Training data comprise both water monomers and large clusters containing 30 molecules, with dataset size, partitioning, and sampling protocol consistent with those used for the other systems. Centroid configurations were generated at 300 K, with A_c and \mathbf{f}_c computed at five temperatures (400, 350, 300, 275, and 250 K) spanning above the boiling point and below the freezing point of water. As shown in Fig. 3a-e, EPIGS accurately learns A_c across all temperatures, achieving RMSEs of approximately 0.1–0.2 meV per atom for the intermediate temperatures and 0.3 meV per atom at the temperature extremes. Similarly strong performance is observed for the quantum entropic term (Fig. 3g-k), with RMSE values of ~ 0.7 meV per atom ($\sim 2\%$ relative

error) across the full temperature range. This level of accuracy is notable given that the training does not include information on the second-derivative with respect to β . Again, validation and test errors closely follow training performance, indicating minimal overfitting. The parity plots also show no systematic deviation between prediction and reference. Furthermore, the model remains predictive outside the training manifold: for a 45-molecule water cluster not included in the training set, EPIGS accurately reproduces both A_c and $\frac{\partial A_c}{\partial \beta}$ over the entire temperature range (Fig. 3f,l).

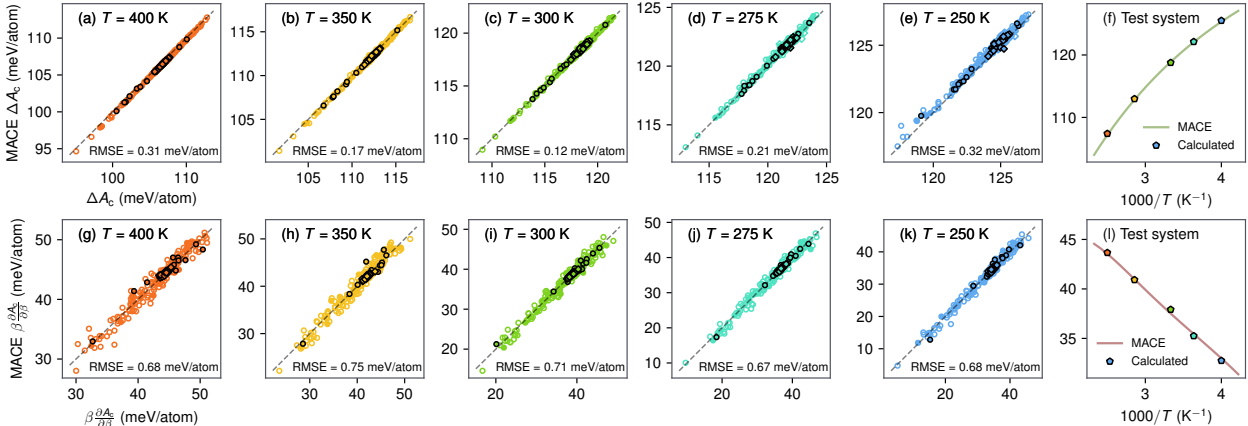


Figure 3: Accuracy and temperature transferability of the EPIGS model for water. (a–f): parity plots for quantum contribution to centroid free energy ΔA_c at five temperatures, with panel (f) showing extrapolation to an unseen 45-molecule test cluster. (g–l): corresponding results for the entropic term $\beta \frac{\partial A_c}{\partial \beta}$. Marker shapes distinguish between monomer (circles) and cluster (diamonds) configurations, while fill styles indicate training (open), validation (solid), and test (solid with black border) sets. RMSE values are computed over the full dataset. Panels (f) and (l) show temperature-dependent predictions to a larger 45-molecule cluster not included in training: solid lines denote continuous MACE predictions, and pentagon markers are reference calculations at discrete temperatures obtained from RPI-FEP and PIMD samplings.

With accurate EPIGS models in hand, we now evaluate their performance for predicting quantum thermodynamic properties. Table 1 compares the classical-to-quantum free energy shifts $\Delta A_c^{q \leftarrow cl}$ computed via EPIGS-TI against the mass-TI benchmark. Across all systems, EPIGS-TI reproduces the mass-TI reference to within 0.25 meV/atom, with most systems having errors below 0.1 meV/atom, which is comparable to the training error of EPIGS itself. The relative errors are below 0.1% for all systems except HCOOD, demonstrating

essentially-exact recovery of the quantum mechanical free energy.

Table 1: Benchmark of EPIGS-TI against mass-TI for classical to quantum free energy shift ($\Delta A^{\text{q-cl}}$). The free energies are reported in meV, while the deviations between EPIGS-TI and mass-TI are normalised by system size (meV/atom). Uncertainties in parentheses apply to the last digit.

System	Mass-TI	EPIGS-TI	Deviation
FAD	908.8(2)	909.86(6)	0.10(2)
HCOOH	457.3(2)	457.51(3)	0.04(3)
HCOOD	392.0(2)	393.26(3)	0.24(3)
HCOO ⁻	246.3(1)	246.54(3)	0.07(3)
Adenine	1402.0(3)	1403.46(8)	0.10(2)
Thymine	1467.2(3)	1468.19(6)	0.06(2)
AT	2864.3(4)	2866.50(10)	0.08(1)
H ₂ O	358.9(2)	359.29(2)	0.12(5)
(H ₂ O) ₄	1449.7(3)	1451.54(4)	0.15(3)

We next consider the more demanding task of predicting NQE contributions to binding and dissociation free energies. These quantities arise from differences between the classical-to-quantum free-energy shifts of related systems. In particular, NQE contributions to binding are small (albeit important), typically on the order of 1–10 meV per molecule, placing stringent demands on model accuracy. EPIGS-TI achieves surprisingly precise agreement within 1 meV of the mass-TI reference for all systems (Table 2). Notably, the water tetramer binding energy is accurately reproduced despite the model being trained with no explicit tetramer data, demonstrating robust transferability across cluster sizes. The results reveal that NQEs strengthen the binding of FAD and the AT base pair, while they destabilise the water tetramer. For formic acid, NQEs lower the pK_a by 3.1 and yield an H→D isotope shift of +1.1, underscoring the significant influence of nuclear quantum fluctuations on acid–base equilibria. The ability of EPIGS to accurately capture delicate NQE contributions satisfies the demanding precision requirements of binding and dissociation thermodynamics, underscoring its broad application potential.

Finally, we address the most challenging application: predicting the enthalpy of vaporisation ΔH_{vap} for liquid water. The challenge is two-fold: EPIGS is trained exclusively on

Table 2: Nuclear quantum contributions to binding and dissociation free energies computed via EPIGS-TI and mass-TI. The binding free energy differences ($\Delta\Delta A_{\text{bind}}^{\text{q}\leftarrow\text{cl}}$) are shown for the formic acid dimer and AT base pair, while the acid dissociation free energy differences ($\Delta\Delta G_{\text{diss}}^{\text{q}\leftarrow\text{cl}}$) are shown for HCOOH and HCOOD, with the pV term evaluated under the ideal gas approximation. All values are in meV, with statistical uncertainties in parentheses applying to the last digit.

Property	Mass-TI	EPIGS-TI	Deviation
$\Delta\Delta A_{\text{bind, FAD}}^{\text{q}\leftarrow\text{cl}}$	-5.8(3)	-5.16(8)	0.6(3)
$\Delta\Delta G_{\text{diss, HCOOH}}^{\text{q}\leftarrow\text{cl}}$	-185.2(2)	-185.12(5)	0.1(2)
$\Delta\Delta G_{\text{diss, HCOOD}}^{\text{q}\leftarrow\text{cl}}$	-119.9(2)	-120.87(5)	-0.9(2)
$\Delta\Delta A_{\text{bind, AT}}^{\text{q}\leftarrow\text{cl}}$	-4.9(6)	-5.1(1)	-0.2(6)
$\Delta\Delta A_{\text{bind, (H}_2\text{O)}_4}^{\text{q}\leftarrow\text{cl}}$	+14.1(5)	+14.38(5)	0.3(5)

clusters yet must predict bulk liquid properties, and accurate ΔH_{vap} requires accurate predictions of not only A_c but also the entropic term. At 300 K, classical MD predicts ΔH_{vap} to be 45.77 kJ/mol. PIMD results show that NQEs raise the internal energy of the liquid more than that of the gas phase due to ZPE in intermolecular vibrational modes arising from the dense hydrogen-bond network, leading to a reduction in ΔH_{vap} by approximately 2.6 kJ/mol relative to classical MD. EPIGS-MD accurately reproduces the PIMD internal energies of both gas-phase and liquid water, yielding $\Delta H_{\text{vap}} = 43.15(4)$ kJ/mol in excellent agreement with the PIMD value (Table 3).

Table 3: Internal energies of gas-phase (U_g) and liquid-phase (U_l) water, and the enthalpy of vaporisation (ΔH_{vap}) at 300 K computed via MD, PIMD, and EPIGS-MD simulations. Internal energies are presented relative to the potential energy of the optimised isolated water molecule. The enthalpy of vaporisation is computed as $\Delta H_{\text{vap}} = U_g - U_l + RT$, assuming ideal gas behaviour and neglecting the liquid molar volume. All values are in kJ/mol, with uncertainties in parentheses applying to the last digit.

	U_g	U_l	ΔH_{vap}
MD	17.36(2)	-25.92(2)	45.77(3)
PIMD	64.49(4)	21.80(3)	43.18(5)
EPIGS-MD	64.45(2)	21.80(3)	43.15(4)

Before concluding, we place EPIGS in the broader context of quantum simulations. The main limitation of EPIGS is that it does not recover bead-resolved nuclear distributions,

and therefore cannot reproduce hydrogen positional distributions for which explicit PIMD remains necessary. Quantum kinetic and potential energy estimators also depend on bead configurations, thus cannot be obtained with the current EPIGS framework. However, based on the relation⁴¹

$$\frac{\langle \widehat{K} \rangle_{U_{\text{RP}}, \mathbf{x}_c}}{m} = \frac{\partial A_c}{\partial m}, \quad (10)$$

it is possible to further extend EPIGS for these two properties. EPIGS is particularly well suited for applications where the primary interest lies in rigorous quantum thermodynamic properties, approximate quantum dynamics via CMD, or quantum heavy-atom configurations, for which the centroid distribution closely approximates the bead distribution. In these cases, EPIGS provides a practical alternative to PIMD at the cost of classical MD. Another key advantage is transferability across system sizes: models trained on small clusters or fragments can be deployed to predict condensed-phase or large-scale behaviour, enabling scalable simulations of complex systems. We also demonstrated reliable temperature-transferable learning of NQEs down to 250 K, with no fundamental limitations for applications at lower temperatures. Therefore, the present work opens a path toward universal pre-trained EPIGS models spanning wide temperature ranges and chemical environments, providing a general and efficient route to incorporate NQEs in large-scale molecular simulations.

4 Conclusions

We have extended the PIGS framework to enable rigorous quantum thermodynamics calculations and temperature-transferable learning of centroid potentials. This advance is made possible by the RPI-FEP approach, which provides an efficient and accurate calculation of the path-integral centroid free energy. Across representative systems, EPIGS models reproduce the training data with sub-meV per-atom errors in A_c and temperature-transferable EPIGS also predicts the temperature derivative of A_c (i.e. quantum entropic term) over the entire temperature range. EPIGS yields precise quantum thermodynamic properties: classical-

to-quantum free energies within 0.2 meV per atom, quantum contributions to binding and dissociation free energies resolved with <1 meV precision, and an enthalpy of vaporisation of liquid water in agreement with PIMD despite being trained exclusively on gas-phase clusters. EPIGS transforms PIGS from a framework primarily used for fast but qualitative simulations of NQEs into a rigorous and accurate efficient simulation approach for quantum thermodynamics simulations at near-classical computational cost, capable of replacing PIMD in many thermodynamic applications.

Conflicts of interest

There are no conflicts to declare.

Acknowledgement

This work is supported by the National Natural Science Foundation of China under grant number 22373021.

References

- (1) Behler, J. Four generations of high-dimensional neural network potentials. *Chem. Rev.* **2021**, *121*, 10037–10072.
- (2) Markland, T. E.; Ceriotti, M. Nuclear quantum effects enter the mainstream. *Nat. Rev. Chem.* **2018**, *2*, 109.
- (3) Fang, W.; Chen, J.; Feng, Y.; Li, X.-Z.; Michaelides, A. The quantum nature of hydrogen. *Int. Rev. Phys. Chem.* **2019**, *38*, 35–61.
- (4) Ceriotti, M.; Fang, W.; Kusalik, P. G.; McKenzie, R. H.; Michaelides, A.; Morales, M. A.; Markland, T. E. Nuclear Quantum Effects in Water and Aqueous

- Systems: Experiment, Theory, and Current Challenges. *Chem. Rev.* **2016**, *116*, 7529–50.
- (5) Benoit, M.; Marx, D.; Parrinello, M. Tunnelling and zero-point motion in high-pressure ice. *Nature* **1998**, *392*, 258–261.
- (6) Chen, B.; Ivanov, I.; Klein, M. L.; Parrinello, M. Hydrogen bonding in water. *Phys. Rev. Lett.* **2003**, *91*, 215503.
- (7) Morrone, J. A.; Car, R. Nuclear quantum effects in water. *Phys. Rev. Lett.* **2008**, *101*, 17801.
- (8) Pamuk, B.; Soler, J. M.; Ramírez, R.; Herrero, C. P.; Stephens, P. W.; Allen, P. B.; Fernández-Serra, M.-V. Anomalous Nuclear Quantum Effects in Ice. *Phys. Rev. Lett.* **2012**, *108*, 193003.
- (9) Bore, S. L.; Paesani, F. Realistic phase diagram of water from “first principles” data-driven quantum simulations. *Nat. Commun.* **2023**, *14*, 3349.
- (10) Li, X.-Z.; Probert, M. I. J.; Alavi, A.; Michaelides, A. Quantum nature of the proton in water-hydroxyl overlayers on metal surfaces. *Phys. Rev. Lett.* **2010**, *104*, 66102.
- (11) Jiang, J.; Gao, Y.; Li, L.; Liu, Y.; Zhu, W.; Zhu, C.; Francisco, J. S.; Zeng, X. C. Rich proton dynamics and phase behaviours of nanoconfined ices. *Nat. Phys.* **2024**, *20*, 456–464.
- (12) Li, X.-Z.; Walker, B.; Michaelides, A. Quantum nature of the hydrogen bond. *Proc. Natl. Acad. Sci. U.S.A.* **2011**, *108*, 6369–6373.
- (13) Fang, W.; Chen, J.; Rossi, M.; Feng, Y.; Li, X.-Z.; Michaelides, A. Inverse Temperature Dependence of Nuclear Quantum Effects in DNA Base Pairs. *J. Phys. Chem. Lett.* **2016**, *7*, 2125–31.

- (14) Rossi, M.; Gasparotto, P.; Ceriotti, M. Anharmonic and Quantum Fluctuations in Molecular Crystals: A First-Principles Study of the Stability of Paracetamol. *Phys. Rev. Lett.* **2016**, *117*, 115702.
- (15) Kapil, V.; Engel, E. A. A complete description of thermodynamic stabilities of molecular crystals. *Proc. Natl. Acad. Sci. U. S. A.* **2022**, *119*, e2111769119.
- (16) Pereyaslavets, L.; Kurnikov, I.; Kamath, G.; Butin, O.; Illarionov, A.; Leontyev, I.; Olevanov, M.; Levitt, M.; Kornberg, R. D.; Fain, B. On the importance of accounting for nuclear quantum effects in ab initio calibrated force fields in biological simulations. *Proc. Natl. Acad. Sci. U. S. A.* **2018**, *115*, 8878–8882.
- (17) Ugur, B. E.; Webb, M. A. Nuclear quantum effects in molecular liquids across chemical space. *Nat. Commun.* **2025**, *16*.
- (18) Masgrau, L.; Roujeinikova, A.; Johannissen, L. O.; Hothi, P.; Basran, J.; Ranaghan, K. E.; Mulholland, A. J.; Sutcliffe, M. J.; Scrutton, N. S.; Leys, D. Atomic description of an enzyme reaction dominated by proton tunneling. *Science* **2006**, *312*, 237–241.
- (19) Pérez, A.; Tuckerman, M. E.; Hjalmarsen, H. P.; Von Lilienfeld, O. A. Enol tautomers of Watson–Crick base pair models are metastable because of nuclear quantum effects. *J. Am. Chem. Soc.* **2010**, *132*, 11510–11515.
- (20) Wang, L.; Fried, S. D.; Boxer, S. G.; Markland, T. E. Quantum delocalization of protons in the hydrogen-bond network of an enzyme active site. *Proc. Natl. Acad. Sci. U. S. A.* **2014**, *111*, 18454–9.
- (21) Rossi, M.; Fang, W.; Michaelides, A. Stability of Complex Biomolecular Structures: van der Waals, Hydrogen Bond Cooperativity, and Nuclear Quantum Effects. *J. Chem. Phys. Lett.* **2015**, *6*, 4233–4238.

- (22) Shen, J.; Du, M.-Z.; Zhang, D. H.; Kapil, V.; Fang, W. On the role of nuclear quantum effects on the stability of peptides. 2025.
- (23) Wahiduzzaman, M.; Walther, C. F. J.; Heine, T. Hydrogen adsorption in metal-organic frameworks: The role of nuclear quantum effects. *J. Chem. Phys.* **2014**, *141*, 064708.
- (24) Liu, M. et al. Barely porous organic cages for hydrogen isotope separation. *Science* **2019**, *366*, 613–620.
- (25) Errea, I.; Calandra, M.; Pickard, C. J.; Nelson, J. R.; Needs, R. J.; Li, Y.; Liu, H.; Zhang, Y.; Ma, Y.; Mauri, F. Quantum hydrogen-bond symmetrization in the superconducting hydrogen sulfide system. *Nature* **2016**, *532*, 81–84.
- (26) Tuckerman, M. *Statistical Mechanics: Theory and Molecular Simulation*; Oxford Graduate Texts; OUP Oxford, 2023.
- (27) Craig, I. R.; Manolopoulos, D. E. Quantum statistics and classical mechanics: Real time correlation functions from ring polymer molecular dynamics. *J. Chem. Phys.* **2004**, *121*, 3368–3373.
- (28) Habershon, S.; Manolopoulos, D. E.; Markland, T. E.; Miller, T. F. Ring-Polymer Molecular Dynamics: Quantum Effects in Chemical Dynamics from Classical Trajectories in an Extended Phase Space. *Annu. Rev. Phys. Chem.* **2013**, *64*, 387–413.
- (29) Cao, J.; Voth, G. A. The formulation of quantum statistical mechanics based on the Feynman path centroid density. I. Equilibrium properties. *J. Chem. Phys.* **1994**, *100*, 5093–5105.
- (30) Voth, G. A. Path-integral centroid methods in quantum statistical mechanics and dynamics. *Advances in Chemical Physics, Vol Xciii* **1996**, *93*, 135–218.
- (31) Shi, Q.; Geva, E. A relationship between semiclassical and centroid correlation functions. *J. Chem. Phys.* **2003**, *118*, 8173–8184.

- (32) Ceriotti, M.; Bussi, G.; Parrinello, M. Nuclear Quantum Effects in Solids Using a Colored-Noise Thermostat. *Phys. Rev. Lett.* **2009**, *103*, 030603.
- (33) Ceriotti, M.; Manolopoulos, D. E. Efficient first-principles calculation of the quantum kinetic energy and momentum distribution of nuclei. *Phys. Rev. Lett.* **2012**, *109*, 100604.
- (34) Markland, T. E.; Manolopoulos, D. E. An efficient ring polymer contraction scheme for imaginary time path integral simulations. *J. Chem. Phys.* **2008**, *129*, 024105.
- (35) Kapil, V.; Behler, J.; Ceriotti, M. High order path integrals made easy. *J. Chem. Phys.* **2016**, *145*, 234103.
- (36) Feynman, R. P.; Hibbs, A. R. *Quantum mechanics and path integrals*, 20th ed.; International series in pure and applied physics; McGraw-Hill: New York, NY, 1995.
- (37) Loose, T. D.; Sahrman, P. G.; Voth, G. A. Centroid Molecular Dynamics Can Be Greatly Accelerated through Neural Network Learned Centroid Forces Derived from Path Integral Molecular Dynamics. *J. Chem. Theory Comput.* **2022**, *18*, 5856–5863.
- (38) Wu, C.; Li, R.; Yu, K. Learning the Quantum Centroid Force Correction in Molecular Systems: A Localized Approach. *Front. Mol. Biosci.* **2022**, *9*, 851311.
- (39) Musil, F.; Zaporozhets, I.; Noé, F.; Clementi, C.; Kapil, V. Quantum dynamics using path integral coarse-graining. *J. Chem. Phys.* **2022**, *157*, 181102.
- (40) Kurnikov, I. V. et al. Neural Network Corrections to Intermolecular Interaction Terms of a Molecular Force Field Capture Nuclear Quantum Effects in Calculations of Liquid Thermodynamic Properties. *J. Chem. Theory. Comput.* **2024**, *20*, 1347–1357.
- (41) Ceriotti, M.; Markland, T. E. Efficient methods and practical guidelines for simulating isotope effects. *J. Chem. Phys.* **2013**, *138*, 14112.

- (42) Habershon, S.; Manolopoulos, D. E. Thermodynamic integration from classical to quantum mechanics. *J. Chem. Phys.* **2011**, *135*, 224111.
- (43) Kleinert, H. *Path Integrals in Quantum Mechanics, Statistics, Polymer Physics, and Financial Markets*; EBL-Schweitzer; World Scientific, 2009.
- (44) Richardson, J. O.; Althorpe, S. C. Ring-polymer molecular dynamics rate-theory in the deep-tunneling regime: Connection with semiclassical instanton theory. *J. Chem. Phys.* **2009**, *131*, 214106.
- (45) Andersson, S.; Nyman, G.; Arnaldsson, A.; Manthe, U.; Jónsson, H. Comparison of Quantum Dynamics and Quantum Transition State Theory Estimates of the H + CH₄ Reaction Rate. *J. Phys. Chem. A* **2009**, *113*, 4468–4478.
- (46) Kästner, J. Theory and simulation of atom tunneling in chemical reactions. *WIREs: Comput. Mol. Sci.* **2014**, *4*, 158–168.
- (47) Richardson, J. O. Ring-polymer instanton theory. *Int. Rev. Phys. Chem.* **2018**, *37*, 171–216.
- (48) Richardson, J. O. Ring-polymer approaches to instanton theory. Ph.D. thesis, Apollo - University of Cambridge Repository, 2012.
- (49) Batatia, I.; Kovács, D. P.; Simm, G. N. C.; Ortner, C.; Csányi, G. MACE: Higher Order Equivariant Message Passing Neural Networks for Fast and Accurate Force Fields. *Adv. Neural Inf. Process. Syst.* 2022; pp 11423–11436.
- (50) Kovács, D. P.; Moore, J. H.; Browning, N. J.; Batatia, I.; Horton, J. T.; Pu, Y.; Kapil, V.; Witt, W. C.; Magdău, I.-B.; Cole, D. J.; Csányi, G. MACE-OFF: Transferable Short Range Machine Learning Force Fields for Organic Molecules. 2025.
- (51) Najibi, A.; Goerigk, L. The Nonlocal Kernel in van der Waals Density Functionals as

an Additive Correction: An Extensive Analysis with Special Emphasis on the B97M-V and ω B97M-V Approaches. *J. Chem. Theory Comput.* **2018**, *14*, 5725–5738.

- (52) Weigend, F.; Ahlrichs, R. Balanced basis sets of split valence, triple zeta valence and quadruple zeta valence quality for H to Rn: Design and assessment of accuracy. *Phys. Chem. Chem. Phys.* **2005**, *7*, 3297.
- (53) Neese, F. Software Update: The ORCA Program System—Version 6.0. *Wiley Interdiscip. Rev. Comput. Mol. Sci.* **2025**, *15*, e70019.